Article

Comprehensive Investigation of Hardness, Wear and Frictional Force in Powder Metallurgy Engineered Ti-6Al-4V-SiC$_p$ Metal Matrix Composites

Adithya Hegde, Rajesh Nayak, Gururaj Bolar, Raviraj Shetty, Rakesh Ranjan and Nithesh Naik

Article

Comprehensive Investigation of Hardness, Wear and Frictional Force in Powder Metallurgy Engineered Ti-6Al-4V-SiC$_p$ Metal Matrix Composites

Adithya Hegde [1] [ID], **Rajesh Nayak** [1,*] [ID], **Gururaj Bolar** [1,*] [ID], **Raviraj Shetty** [1] [ID], **Rakesh Ranjan** [2] [ID] **and Nithesh Naik** [1] [ID]

1   Department of Mechanical and Industrial Engineering, Manipal Institute of Technology, Manipal Academy of Higher Education, Manipal, Udupi 576104, Karnataka, India; adithya.hegde@learner.manipal.edu (A.H.); rr.shetty@manipal.edu (R.S.); nithesh.naik@manipal.edu (N.N.)
2   Department of Information Technology, ABES Engineering College, Ghaziabad 201009, Uttar Pradesh, India; rakesh.ranjan@abes.ac.in
*   Correspondence: nayak.raj@manipal.edu (R.N.); gururaj.bolar@manipal.edu (G.B.)

Abstract: Metal matrix composites (MMCs) have achieved significant attention in engineering applications because of their exceptional properties, like increased strength-to-weight ratiosand resistance to wear. However, their manufacturing processes pose challenges for industries, such as oxidation, porosity, and chemical reactions. To address these challenges, this study investigates the processing and sintering (500 °C) of Ti-6Al-4V-SiC$_p$ composites and their mechanical properties, particularly hardness, wear and frictional force using a statistical approach. The main objective of this research is to identify optimal processing conditions for Ti-6Al-4V-SiC$_p$ composites that yield maximum hardness, minimal wear and frictional force. Thisstudy varies three key parameters, namely compaction pressure (Ton/sq.inch), SiC (wt.%), and PVA binder (wt.%) using Taguchi's design of experiments (TDOE). Further, the response surface methodology (RSM) is used to develop second-order models to predict the output values under different processing conditions, by correlating with the values obtained from TDOE. The results indicate that the most significant influence on the output is exerted by SiC (wt.%), followed by PVA binder (wt.%) and compaction pressure (Ton/sq.inch). To achieve higher hardness with minimal wear and frictional force during processing, SiC$_p$ (15 wt.%), compaction pressure (4 Ton/sq.inch), and PVA binder (3 wt.%) arerecommended. Finally, microstructural analysis using (SEM) scanning electron microscope images, optical macrographs and (AFM) atomic force microscopy revealed that the inclusion of 15 wt.% SiC$_p$ resulted in improved hardness, wear and frictional force compared to 20 wt.% SiC$_p$. In conclusion, this study provides valuable insights into optimizing the processing parameters of Ti-6Al-4V-SiC$_p$ samples, enabling the production of materials with enhanced hardness and wear resistance.

Keywords: surface metallurgy; Taguchi's design of experiments (TDOE); Ti-6Al-4V; SiC; response surface methodology (RSM); hardness; wear; frictional force; atomic force microscopy; scanning electron microscopy (SEM)

1. Introduction

Metal matrix composites (MMCs) represent a novel class of materials wherein the properties of a metal matrix are enhanced through the incorporation of a ceramic reinforcement [1–7]. By integrating metallic matrices (known for their high ductility and high toughness) along with ceramic material reinforcements (possessing high strength and high modulus), MMCs exhibit improved compression and shear strength, elevated working temperature, enhanced electrical conductivity, density, and coefficient of thermal expansion [8–33]. Consequently, MMCs have found widespread application in high-performance fields, such as recent advancements in the automotive sector and aircraft engines. The

inclusion of ceramics as either fiber or particle reinforcement within the titanium alloy matrix leads to enhanced mechanical, thermal, and tribological properties [34]. Continuous fibers notably augment strength in the direction of fiber alignment, particularly at high temperatures [35]. The interaction between ceramics like silicon carbide and titanium results in the formation of brittle silicide phases, TiCx, and Ti5Si3Cx [36]. Presently, silicon carbide particles are commonly employed to reinforce titanium alloys and titanium aluminide matrix phases [37].

Titanium matrix composites (TMCs) with discontinuous or particle reinforcement are relatively easier to manufacture and exhibit nearly isotropic characteristics. As a result, particulate-reinforced TMCs have garnered significant interest for structural applications [38]. Extensive research has been dedicated to expanding the scope of applications and production methods for these materials. Among the ceramics investigated as reinforcements for titanium alloys are titanium carbide (TiC), titanium dioxide (TiO_2), titanium boride (TiB) and titanium diboride (TiB_2), as well as silicon dioxide (SiO_2), silicon carbide (SiC) and silicon nitride (SiN). SiC has emerged as the most desirable material for reinforcement [39]. The mechanical properties of MMCs, such as a high strength-to-weight ratio and thermal–electrical conductivity, can be further improved by increasing the density of produced TMCs [40].

Powder metallurgy (PM) stands out as a highly versatile manufacturing technique, as it enables the creation of intricately shaped, high-quality products with tight tolerances. PM facilitates the production of near-net-shaped, highly functional components that are less susceptible to faults or porosity [41]. To study the manufacturing processes comprehensively, statistical techniques like Taguchi's design of experiments are employed. This statistical method involves the creation of mathematical models through experimental testing to predict potential outcomes based on input factors [42,43]. Analysis of variance (ANOVA) is employed to examine the contribution percentage of process input factors [44,45]. In this context, response surface methodology is a widely used experimental design for optimization, while evaluating the effects of multiple parameters and the effect of their interactions on multiple response (output) parameters [46,47].

In this field despite of extensive research efforts, several critical knowledge gaps persist. One aspect is the exploration of alternative ceramic reinforcements beyond the widely utilized silicon carbide (SiC), including titanium carbide (TiC) and titanium dioxide (TiO_2). Investigating their material properties and integration feasibility within composites is crucial for diversifying available materials. Additionally, there is a need for comprehensive studies optimizing powder metallurgy (PM) parameters for Ti-6Al-4V-SiCp composites, and a deeper understanding of how compression pressure, SiC content, and PVA binder Content interact to influence hardness. This research aims to address these gaps while striving to enhance the performance and application scope of these advanced composites. The present work aims to process Ti-6Al-4V-SiC$_p$ composites using the powder metallurgy technique and investigate the influence of input process parameters, such as compression pressure (MPa), SiC content (wt.%), and PVA binder content (wt.%), on hardness through the combination of TDOE and RSM.

2. Materials and Methods/Methodology

In this experimentation, Ti-6Al-4V (titanium alloy) and SiC (silicon carbide) with a particle size of 100 μm along with binder powder (PVA) polyvinyl alcohol have been sourced from Paraswamani Metals, Mumbai. The chemical composition of titanium alloy and silicon carbide are presented in Table 1 as well as in Table 2. A double action split-die has been designed for processing of titanium silicon carbide composites. The matrix and reinforcement powders are mixed along with PVA binder and are ball milled for 1 h to achieve homogenous mixing of materials. Further, the mixture is compacted using modified compacting machine setup. Figure 1 portrays the Flowchart of the experimentation process. The factors and levels selected for compacting the powders are presented in Table 3. The green compacted samples are then sintered at 500 °C for 2 h in a muffle furnace. The

samples are characterized for Brinell hardness value using Analog B 3000 (H) Hardness Testing Equipment. Indentation load (10 kgf) with dwell time (20 s) to obtain indentation on the surface using steel ball of diameter (10 mm). The hardness is found out using equation given below.

$$HBW = \frac{2P}{\pi D \left(D - \sqrt{(D^2 - d^2)} \right)} \tag{1}$$

where P is the applied force (kgf); D is the diameter of the indenter ball in mm; d is the mean diameter of the indentation in mm (it ismeasured twice, typically left–right and top–bottom).

Table 1. Ti-6Al-4V constituents [48].

Constituents	V	Al	O	Fe	N	C	H	Y	Ti
wt.%	4	6.1	0.11	0.16	0.01	0.02	0.0011	0.0013	Bal

Table 2. SiC constituents [48].

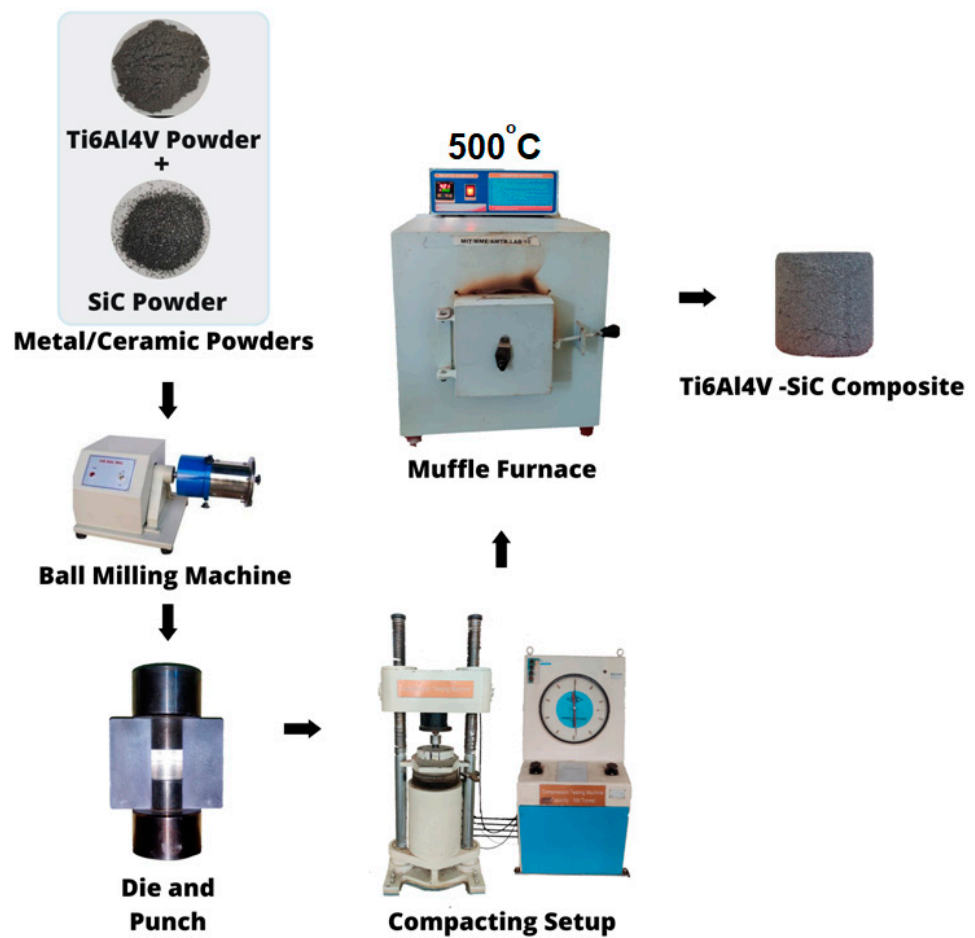| Compound	Si	Al_2O_3	C	Fe_2O_3	SiO_2	CaO	S	P	SiC
wt.%	1.43	0.24	1.18	0.67	0.8	0.15	0.05	0.33	Bal

Figure 1. Flowchart of processing and characterization of titanium silicon carbide composite.

Table 3. TDOE factors and levels.

Levels	(A) SiC (wt.%)	(B) Compression Pressure (Ton/sq.inch)	(C) PVA Binder (wt.%)
1	10	3	3
2	15	4	4
3	20	5	5

Contact area information is calculated using the given equation

$$A = \pi * \left(\frac{D^2}{2} \right) \tag{2}$$

where D is the diameter of the spherical indenter.

Further, for measuring wear and frictional force, specimens of 8 mm diameter with 30 mm length were chosen as per ASTM G99-05 standards. Input parameters such as sliding velocity (1 m/s), load (10 N) and sliding distance (1000 m) are taken constant. The pins were made even with P-1200 grade abrasive paper to ensure they had the sameroughness. The test duration, weight to apply, sliding speed, and sliding distance by conducting a pilot study. An accurate electronic balance is used to measure the pin's starting weight (at least 0.0001 g). After putting the pin in the holder, weight is added using a lever. Once the test is conducted, the pin is weighed again with the same balance and weight lost is calculated. The test has been conducted three times to make sure the consistency of the results. The specific rate of wear (K) was calculated using below equation.

$$K = \frac{\Delta W}{\rho L D} \tag{3}$$

Further, Taguchi's L_{27} orthogonal array is formulated using MINITAB 15 to optimize the input process parameters. Finally, RSM (Table 4) is used to establish pragmatic interaction among the process parameters selected. In this study, sets of experiments are conducted in accordance with the experimental design matrix and sorted using the standard ordering.

Table 4. RSM factors and levels.

| Levels	(A) SiC (wt.%)	(B) Compression Pressure (Ton/sq.inch)	(C) PVA Binder (wt.%)
1	10	3	3
2	20	5	5

3. Results and Discussion

After homogeneous distribution of silicon carbide (SiC) reinforcement with a titanium alloy (Ti-6Al-4V) matrix during processing, a TDOE and RSM approach for predicting hardness, wear and frictional force has been discussed.

3.1. Hardness Analysis

Hardness is an important criterion to consider while fabricating the titanium composites. Figure 2 presents the experimental details of hardness of samples processed under differentSiC (wt.%), compression pressure (Ton/sq.inch), PVA binder (wt.%). From the figure (Figure 2), it is observed that the hardness value increased at 15 wt.% SiC, compared to 10 wt.% SiC and 20 wt.% SiC. The 15 wt.% SiC content plays a crucial role in enhancing the overall hardness as SiC is known for its hardness and strength. Its uniform distribution within the matrix acts as effective barriers to impede dislocation movements during deformation and thus increasing the strength and hardness of the composite. Comparatively, with lower SiC content (10wt.%), there is not enough reinforcement to significantly improve the mechanical properties. Conversely, a higher SiC content (20 wt.%) leads to

particle agglomeration, reducing uniformity and causing stress concentration points that further lowers the hardness. Additionally, the 4 Ton/sq.inch compaction pressure helps in achieving optimal particle packing and reduced porosity, resulting in improved mechanical properties. Lower compaction pressures (3 Ton/sq.inch) may lead to incomplete particle bonding and porosity, whereas higher pressures (5 Ton/sq.inch) could cause particle fracture and damage, both negatively impacting the hardness. Lastly, the 3 wt.%PVA binder provides the necessary binding strength during the compaction process, aiding in maintaining the structural integrity of the composite. However, excessive binder content may lead to increased porosity and reduced hardness. The increase in hardness at 15 wt.% SiC is due to its uniform distribution within the matrix, impeding dislocation movement during deformation, while lower SiC content lacks sufficient reinforcement and higher SiC content leads to particle clustering, causing stress concentration points that reduce hardness. Thus, the observed combination of SiCwt.%, compaction pressure, and PVA binder wt.% demonstrates a balanced microstructure, contributing to the highest hardness observed in the MMC.
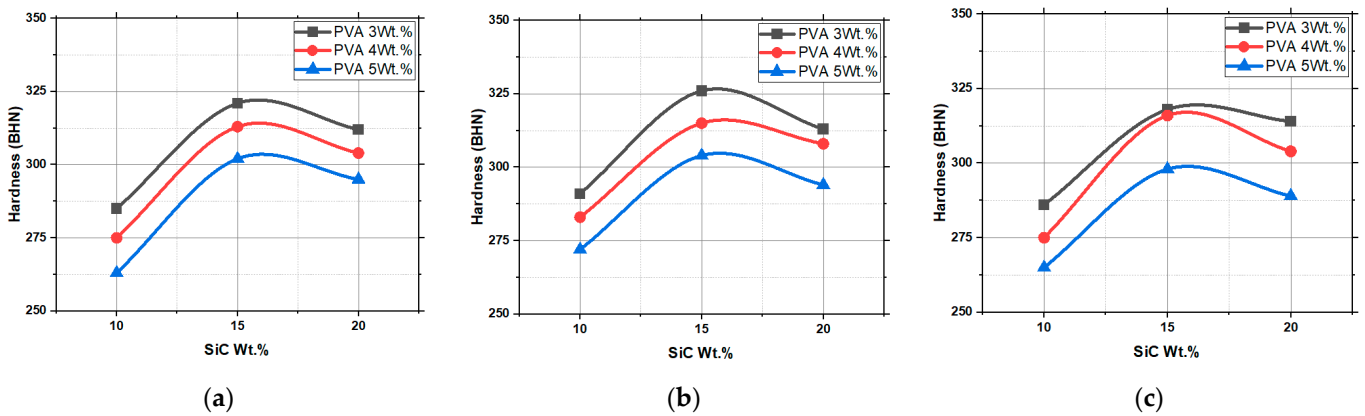
Figure 2. Variation inhardness (BHN) under varying SiC$_p$ (wt.%) and PVA binder (wt.%) with compaction pressure; (**a**) 3 Ton/sq.inch; (**b**) 4 Ton/sq.inch; (**c**) 5 Ton/sq.inch.

From Figure 3, i.e., main effects plot of hardness, it can be clearly observed that the selection of SiC$_p$ (15 wt.%), compaction pressure (4 ton/sq. inch) and PVA binder (3 wt.%) as the optimum combination of parameters to obtain the highest hardness (BHN) value during fabrication of Ti-6 Al-4V-SiC$_p$ composites.
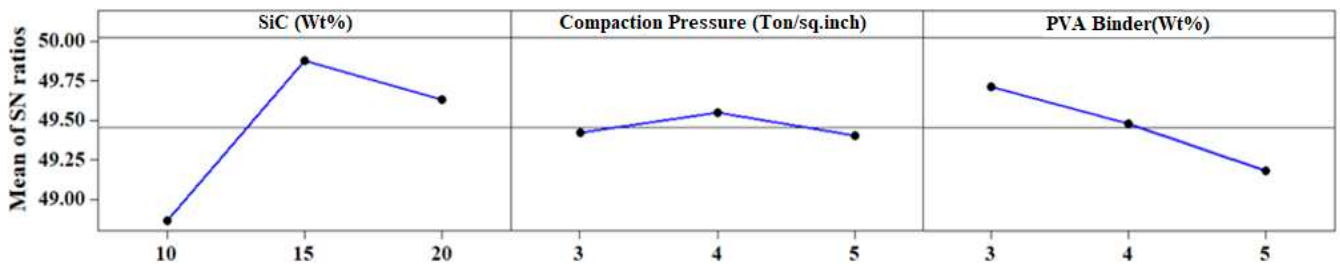
Figure 3. Main effects plot for hardness (BHN).

ANOVA indicates that SiC (wt.%) is one of the prominent factors considered while fabricating Ti-6Al-4V-SiC$_p$ composites. Among the contribution percentage (p%) of the different selected factors (Table 5) for hardness, SiC (wt.%) (A) has the largest contribution of around 77.99%. It can be seen that PVA binder (C) (19.87%), compaction pressure (B) (1.85%), and interactions A × B, A × C, (0.22%, 0.15%) had less significance on hardness both statistically and physically. The interactions (B × C) do not provide statistical or physical significance to the hardness.

Table 5. ANOVA (analysis of variance) for SN ratios.

Source	Deg. F	Seq. SS	Adj. SS	Adj. MS	F	p	p%
A	2	5.03901	5.03901	2.51950	1035.67	0.000	77.99
B	2	0.11244	1.28403	0.05622	23.11	0.000	1.85
C	2	1.28403	1.28403	0.64202	263.91	0.000	19.87
A × B	4	0.02969	0.02969	0.00742	3.05	0.084	0.22
A × C	4	0.01975	0.01975	0.00494	2.03	0.183	0.15
B × C	4	0.00130	0.00130	0.00033	0.13	0.965	0.009
Residual error	8	0.01946	0.01946	0.00243			
Total	26	6.50569					

Equation (4) presents a second-order differential equation for hardness, which is expressed as a function of input processing parameters (SiC wt.%, compaction pressure and PVA wt.%).

$$\text{Hardness (BHN)} = 39.2029 + 27.9847\,A + 27.6647\,B + 5.01471\,C - 0.838824\,A^2 - 2.97059\,B^2 - 1.97059\,C^2 - 0.2\,AB + 0.15\,AC - 0.25\,BC \tag{4}$$

Analysis is carried out at a significance level of 5% while the level of confidence is at 95%. The results of ANOVA clearly indicate that the 'F' table value (Table 6) is less than the calculated value of 'F' ($F_{(0.05,9,9)} = 329.4$). Thus, the developed equation is considered adequate.

Table 6. ANOVA for response function of the hardness.

Source	Deg.F	Seq. SS	Adj. MS	F	P
Regression	9	4991.39	554.599	329.4	0.000
Residual Error	9	15.15	1.684		
Total	18	1.89670			

For each of the response surfaces, contour and surface plots are plotted at different SiC (wt.%) and PVA binder (wt.%) with compression pressure (4 Ton/sq.inch) is plotted (Figure 4). These response contours and surface plot are used to predict hardness (BHN) at any area. It is clear from the figure that the maximum hardness ranges from 14 to 18 (wt.%) of SiC with 3–3.5 (wt.%) of PVA binder.
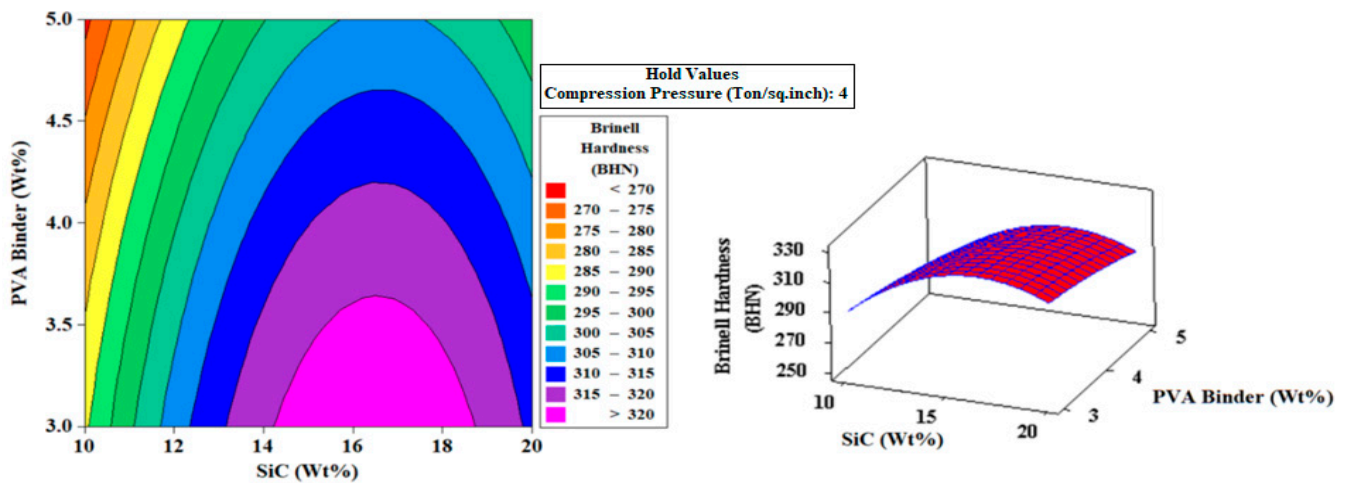

Figure 4. Hardness contour plot and surface plot in SiC (wt.%)-PVA binder (wt.%) at 4 Ton/sq.inch.

Figure 5 presents the microstructure of titanium composites under varying combination of input parameters. From the analysis, it was concluded that Ti-6Al-4V reinforced with 10 wt.% of SiC_p had more void formation compared to 15 wt.% and 20 wt.% of SiC_p, respectively. Further, 15 wt.% of SiC_p forms an α-phase of titanium, which further increases the hardness compared to 20 wt.% of SiC_p. Further, cracks are formed when SiC_p wt.% is increased, because of the decrease in interlocking and bond strength.

(a)   **(b)**   **(c)**
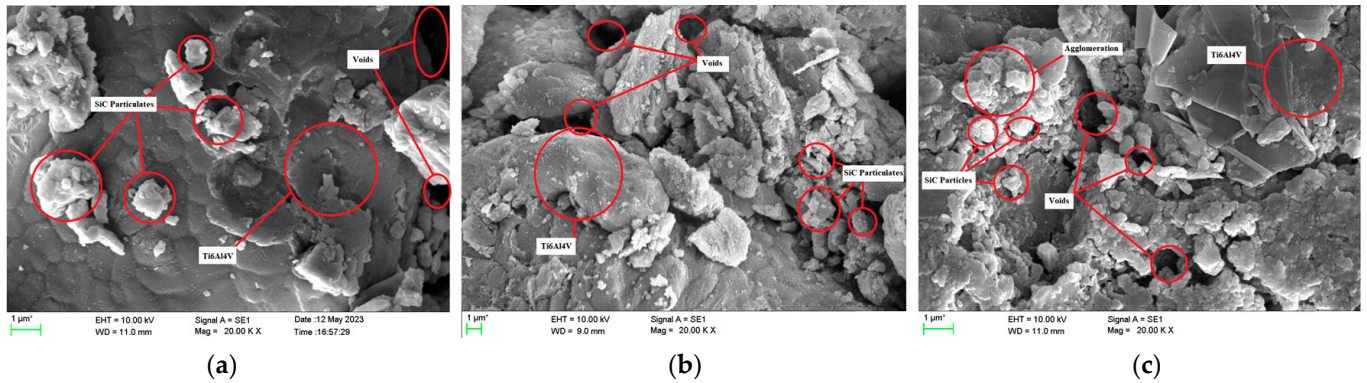
Figure 5. Microscopic images of processed Ti-6Al-4V-SiCp samples with (**a**) SiC wt.% (10 wt.%), (**b**) SiC wt.% (15 wt.%), and (**c**) SiC wt.% (20 wt.%) while PVA binder wt.% (3wt.%) and compression pressure (4 Ton/sq. inch) are kept constant.

The RSM predicted values of hardness (BHN) are verified by comparing with TDOE hardness (BHN) values. For 27 trials, the observed average error was 0.69%, which concludes that the estimation is accurate. Figure 6 presents the verification test results for hardness (BHN).
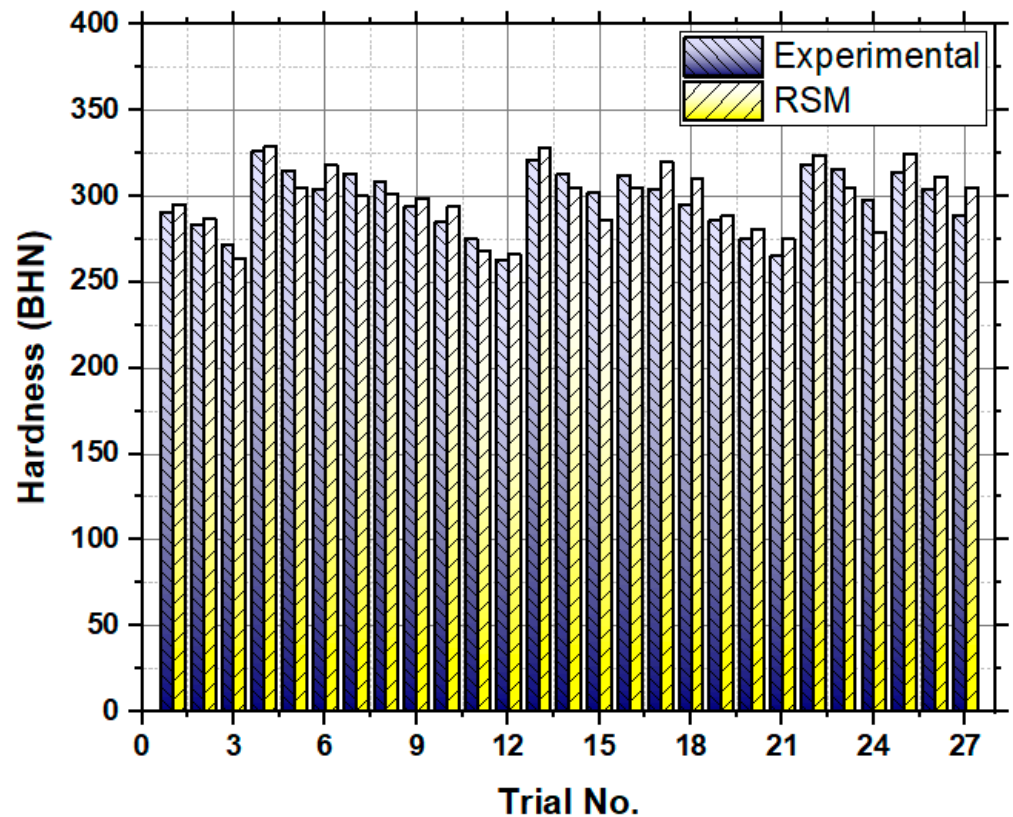
Figure 6. Verification of RSM prediction of hardness (BHN).

3.2. Wear Analysis

Wear in materials refers to the gradual loss of material due to the mechanical action of another surface rubbing against it. The wear rate (mg/min) of composite sample during Pin on Disc Wear Testing process can be significantly influenced by several processing parameters such as SiC wt.%, compaction pressure (Ton/sq.inch) and PVA binder wt.%. The SiC wt.% affects the atomic structure of the composite, where increasing the SiC wt.% can lead to better dispersion of the particles of reinforcement, increased hardness and stiffness of the composite, and reduced material loss due to wear. Figure 7 presents the experimental results of wear (mg/m) under constant load (10 N) sliding velocity (1 m/s), along with sliding distance (1000 m). A PVA binder content of 3 wt.% results in minimal wear due to reduced porosity in titanium silicon carbide composites, while 4 wt.% yields intermediate wear, and 5 wt.% leads to elevated wear levels, correlating with increased porosity as PVA evaporates during the powder metallurgy process, leaving behind pores that influence wear resistance. At the micro level, when SiC content is lower (10 wt.%), the composite has less reinforcement, making it more susceptible to wear as the softer titanium matrix is exposed. Similarly, at higher compaction pressures (5 Ton/sq.inch), the higher densification of the composite might lead to increased wear, as the interfaces between the Ti-SiC particles become more prone to damage due to the higher contact stresses during sliding. However, at the intermediate SiC content (15 wt.%), the microstructure is optimized, providing a balanced combination of reinforcement and matrix properties. This leads to improved wear resistance, as the SiC particles can act as load-bearing elements, distributing the applied load and reducing wear on the titanium matrix. Additionally, a moderate compaction pressure (4 Ton/sq.inch) creates a well-bonded structure with fewer defects, resulting in better wear resistance compared to lower compaction pressures. The wear rate during Pin on Disc Wear Testing is significantly influenced by SiC wt.%, compaction pressure, and PVA binder wt.%; higher SiC wt.% enhances dispersion, hardness, and stiffness, reducing wear, while lower SiC content makes the composite more prone to wear; increased compaction pressure may lead to higher wear due to increased contact stresses, but at an intermediate SiC content of 15 wt.%, a balanced microstructure improves wear resistance by distributing load through SiC particles, and moderate compaction pressure reduces defects, enhancing wear resistance compared to lower pressures.
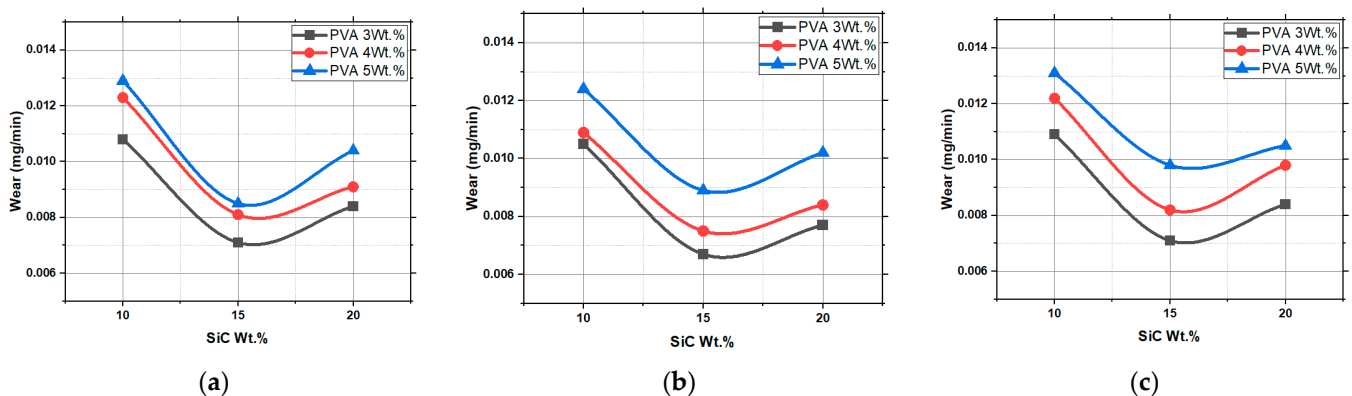
Figure 7. Variation inwear (mg/min) under varying SiC_p (wt.%) and PVA binder (wt.%) with compaction pressure; (**a**) 3 Ton/sq.inch; (**b**) 4 Ton/sq.inch; (**c**) 5 Ton/sq.inch.

Figure 8 presents the worn surface of Ti6Al4V-SiCp composites after the experimentation. In the composite specimen with 10 wt.% SiC, a surface with visible signs of wear is observed. The wear patterns are more pronounced compared to the samples with higher SiC content. The wear mechanisms in this sample are dominated by abrasive wear, where the softer titanium matrix is subjected to localized abrasion from the harder SiC particles. Similarly, the composite sample with 20 wt.% SiC shows a distinctive wear pattern compared to the other two samples. With the highest SiC content, this sample exhibits a more

textured and rough surface due to the increased presence of hard SiC particles. However, despite the higher SiC content, wear at this level is not high compared to the 10 wt.% SiC sample. The SiC particles play a crucial role in enhancing wear resistance, but an excessively high SiC content leads to increased abrasive wear and potential particle agglomeration. However, the composite specimen with 15 wt.% SiC exhibits a more uniform and smoother surface compared to the other samples. At this intermediate SiC content, the wear behavior shows a transition from predominantly abrasive wear to a combination of abrasive and adhesive wear. The SiC particles are load-bearing elements which reduce the wear on the titanium matrix, resulting in a more balanced wear profile.
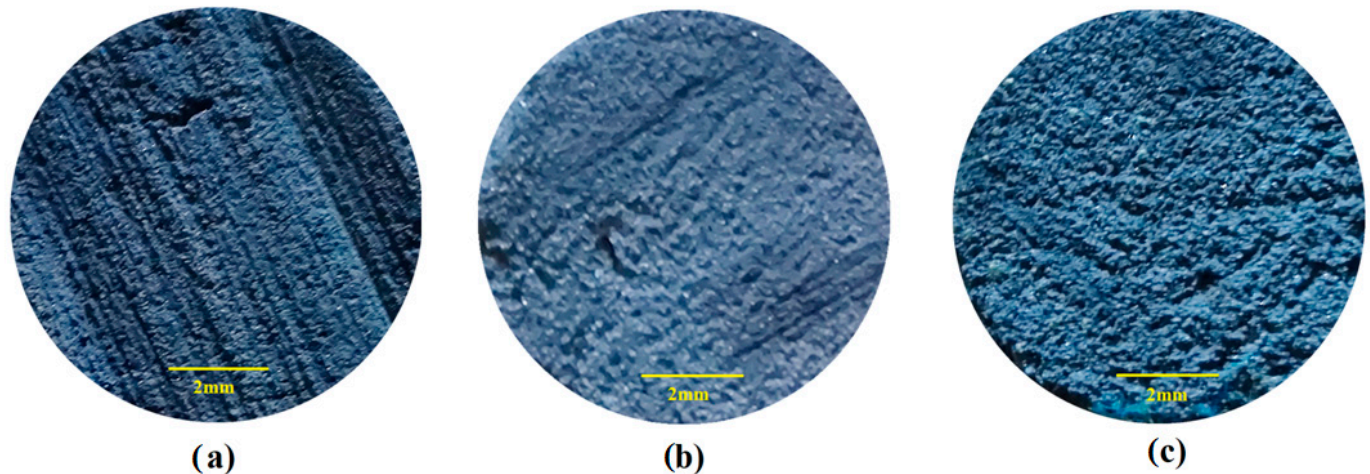

Figure 8. Optical macrograph of worn surface of Ti-6Al-4V-SiCp composites under different processing conditions (**a**) SiC wt.%(10 wt.%), (**b**) SiC wt.% (15 wt.%), and (**c**) SiC wt.% (20 wt.%) at PVA binder wt.% (3 wt.%) and compression pressure (4 Ton/sq. inch) kept constant.

Figure 9 presents the atomic force microscope (AFM) image of theworn surface with different SiC wt.%. For the sample with 10 wt.% SiC, the AFM image displays a surface with noticeable wear tracks, increased surface roughness, and abrasive wear debris.The presence of harder SiC particles likely caused localized ploughing and scratching of the titanium matrix, leading to the formation of wear tracks. The surface roughness looks pronounced compared to samples with higher SiC content, indicating higher wear rates and a less uniform surface. Moreover, the AFM images suggest the presence of wear debris and possible particle agglomeration, shedding light on the dominant wear mechanisms at 10 wt.% SiC. Further, for the sample with 20 wt.% SiC, the AFM image exhibits distinct wear patterns due to an increased presence of SiC particles. The higher SiC content leads to a textured surface, with possible indications of SiC particle agglomeration. AFM analysis provides detailed information about the distribution and arrangement of SiC particles on the surface, which influences the wear behavior. However, despite the higher SiC content, the AFM image shows relatively fewer wear features compared to the 10 wt% SiC sample, suggesting improved wear resistance achieved with 20 wt.% SiC samples. Finally, the AFM image of 15 wt.% SiC sample reveals a smoother and more controlled surface. The wear behavior at this intermediate SiC content achieves a balance between abrasive and adhesive wear mechanisms, resulting in a relatively more uniform wear profile and reduced surface roughness. The presence of SiC particles contribute to load-bearing and wear reduction effects, resulting in shallower wear tracks and less pronounced surface features in the AFM image.

The main effects plot (Figure 10) for wear indicates that the selection of SiCp (15 wt.%), compaction pressure (4 ton/sq. inch) and PVA binder (3 wt.%) results in the best combination of input parameters to derive least wear values during processing of titaniumcomposites.
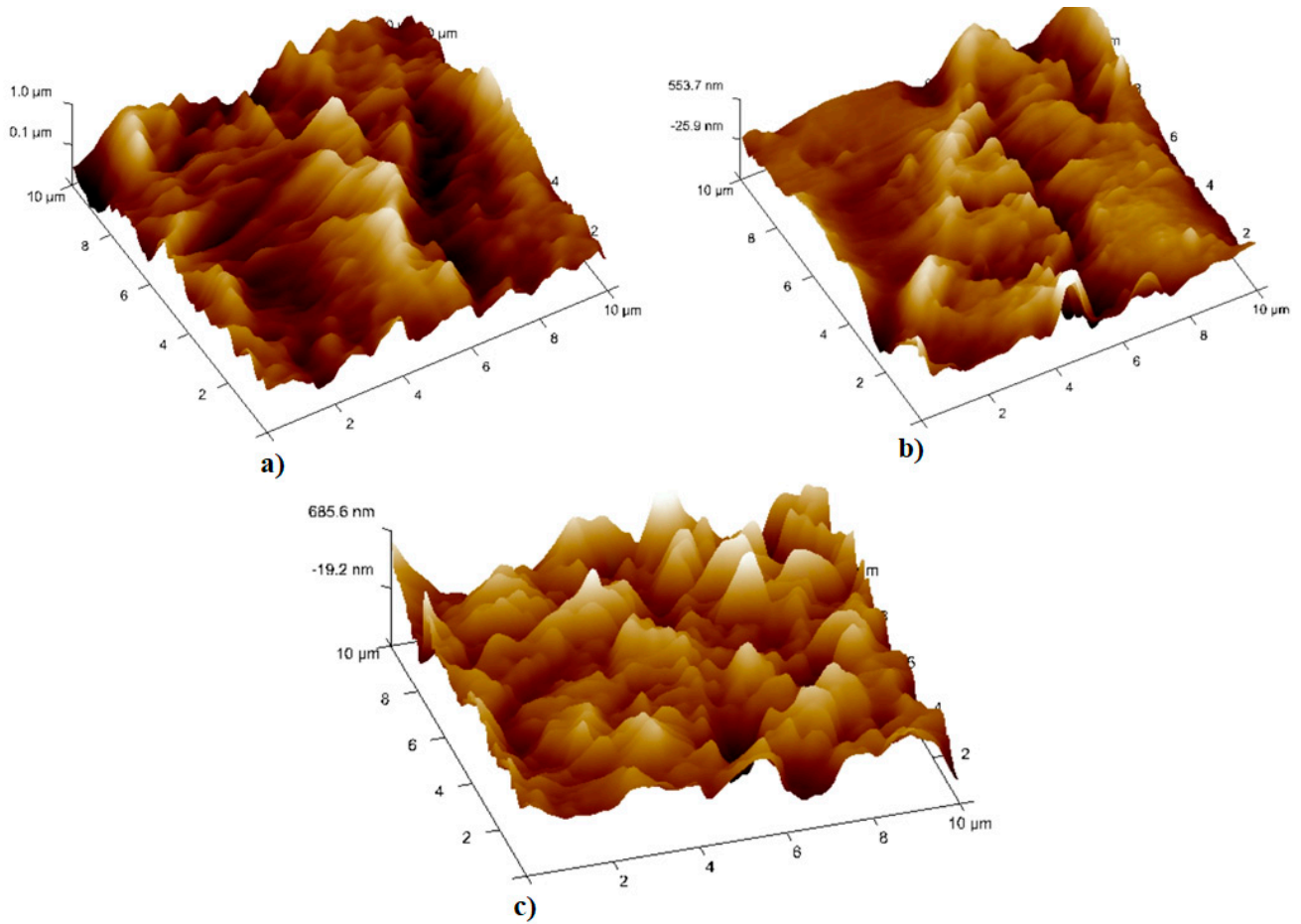
Figure 9. Atomic force microscopic images of worn surface of the composite specimen with; (**a**) SiC wt.%(10 wt.%), (**b**) SiC wt.% (15 wt.%), and (**c**) SiC wt.% (20 wt.%) at PVA binder wt.% (3 wt.%) and compression pressure (4 Ton/sq. inch) kept constant.
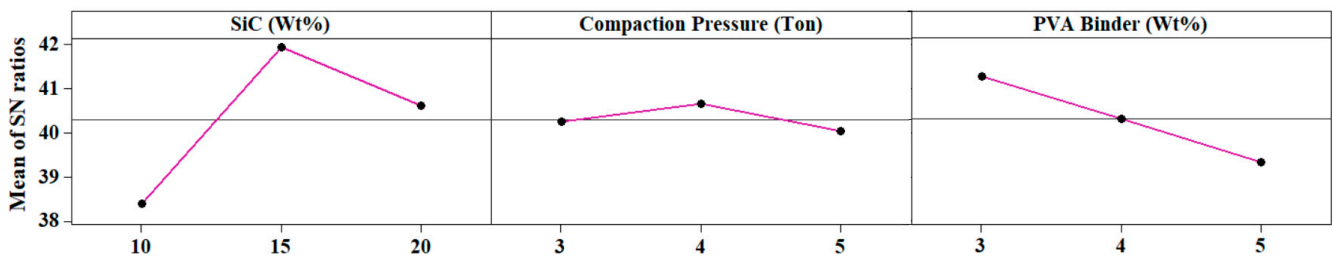
Figure 10. Main effects plot for wear (mg/min).

Results of ANOVA deduce that SiC (wt.%) is a prominent parameter which needs to be taken into consideration while processing titanium composites. Among the percentage of contribution (P%) of the various parameters (Table 7) for wear, SiC (A) has the largest contribution of around 76.99%. It can be seen that PVA binder (C) ($p = 19.76\%$), compaction pressure (B) ($p = 2.072\%$), and interactions A × B, A × C, ($p = 0.101\%$, 0.899%) had less physical and statistical significance on wear. The interactions (B × C) are not of any physical or statistical significance.

Table 7. ANOVA (analysis of variance) for SN ratios.

Source	Deg.F	Seq. SS	Adj. SS	Adj. MS	F	p	p%
A	2	0.000074	0.000074	0.000037	882.99	0.000	76.99
B	2	0.000002	0.000002	0.000001	23.80	0.000	2.072
C	2	0.000019	0.000019	0.000010	226.42	0.000	19.76
A × B	4	0.000000	0.000000	0.000000	1.16	0.397	0.101
A × C	4	0.000002	0.000002	0.000000	10.30	0.003	0.899
B × C	4	0.000000	0.000000	0.000000	0.88	0.516	0.076
Residual Error	8	0.000000	0.000000	0.000000			
Total	26	0.000098					

Equation (5) presents the second-order differential equation for representing the wear (mg/min) which can also be given as a function of input processing parameters such as (A) SiC (wt.%), (B) compression pressure (Ton/sq. inch) and (C) PVA binder (wt.%).

$$\text{Wear (mg/min)} = 0.0473 - 0.00370192\,A - 0.00424972\,B - 0.00126972\,C + \\ 0.000109133\,A^2 + 0.000478329\,B^2 + 0.000178329\,C^2 + 0.00000093099\,A \times B + \\ 0.00000293\,A \times C + 0.000009654\,B \times C \tag{5}$$

Analysis is carried outat a significance level of 5% while the level of confidence is at 95%. The results of ANOVA clearly indicate that the 'F' table value (Table 8) is less than the calculated value of 'F' ($F_{(0.05,9,9)} = 109.2$). Thus, the developed equation is considered adequate.

Table 8. ANOVA for response function of the wear.

Source	Deg.F	Seq. SS	Adj. MS	F	P
Regression	9	0.000072	0.000008	109.20	0.000
Residual Error	9	0.000001	0.000000		
Total	18	0.000073			

For each of the response surfaces, contour and surface plots are plotted at different SiC (wt.%) and PVA binder (wt.%) with compression pressure (4 Ton/sq.inch) is plotted (Figure 11). These response contours and surface plot are used to predict wear(mg/min) at any area. It is clear from the figure that the minimum wear ranges from 16 to 18 (wt.%) of SiC with 3.5–5 (wt.%) of PVA binder.
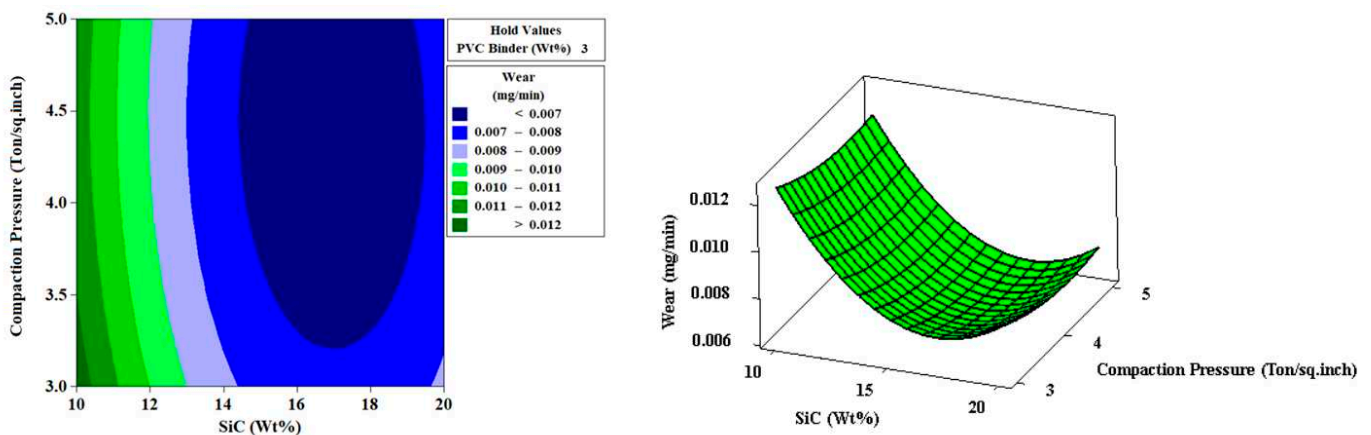

Figure 11. Contour plot and surface plot for wear (mg/min).

The RSM predicted values of wear (mg/min) are verified by comparing with TDOE values. For 27 trials, the observed average error was 1.21%, which concludes that the estimation is clearly accurate. Figure 12 presents the verification test results for wear(mg/min).
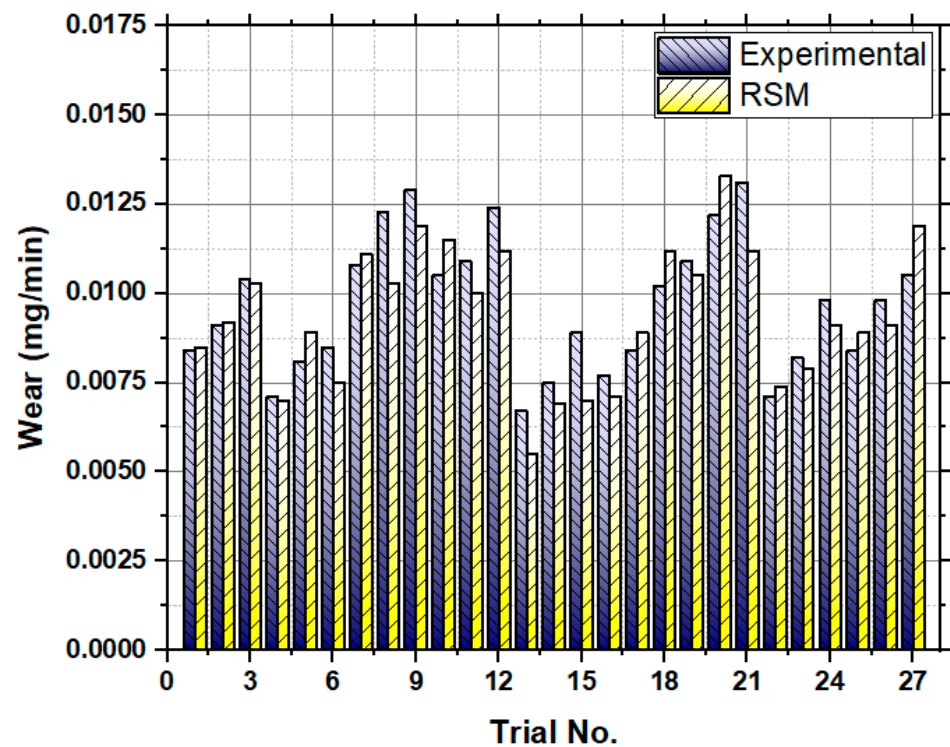

Figure 12. Verification of RSM prediction of wear.

3.3. Frictional Force Analysis

Frictional force is a measure of the resistance encountered when two surfaces slide against each other. The frictional force (N) of composite sample during the Pin on Disc Wear Testing process can be significantly influenced by several processing parameters such as SiC wt.%, compaction pressure (Ton/sq.inch) and PVA binder wt.%. Frictional force, on the other hand, is a measure of the resistance encountered when two surfaces slide against each other. In the Ti6Al4V-SiCp composites, frictional force is influenced by the interfacial behavior between the TiSiC particles and the titanium matrix. At higher SiC contents (20 wt.%), there isa higher tendency for agglomeration of SiC particles, leading to uneven distribution and increased frictional resistance during sliding. Similarly, at higher binder content (5 wt.% PVA), excess binder material coats the SiC particles, reducing their direct interaction with the titanium matrix and increasing the contact area between the binder and the counter-surface, resulting in higher frictional force. Conversely, at intermediate SiC content (15 wt.%) and moderate PVA binder content (3 wt.%), the composite exhibits the best balance between load-bearing capacity, interfacial adhesion, and wear resistance. This combination could reduce the frictional force during sliding due to optimized microstructural features and better load distribution, resulting in lower frictional losses. The presence of SiC particles as reinforcement enhances the hardness as well as resistance to wear of the composite. Further, the moderate compaction pressure promotes a well-bonded microstructure with a balanced distribution of SiC particles, minimizing defects and ensuring effective load transfer. Finally, the appropriate PVA binder content allows for good interfacial adhesion between the particles and the titanium matrix, leading to efficient stress transfer and reduced frictional losses. Figure 13 presents the experimental results of frictional force (N) under constant sliding velocity (1 m/s), load (10 N) and sliding distance (1000 m). Thus, the frictional force during Pin on Disc Wear Testing in Ti6Al4V-SiCp composites is significantly affected by SiC content and PVA binder content;

higher SiC content leads to particle agglomeration and increased friction, while higher PVA binder content reduces SiC-titanium matrix interaction, resulting in greater friction, but at an intermediate SiC content and moderate PVA binder content, a well-balanced microstructure reduces frictional force through optimized load distribution and interfacial adhesion, minimizing frictional losses.
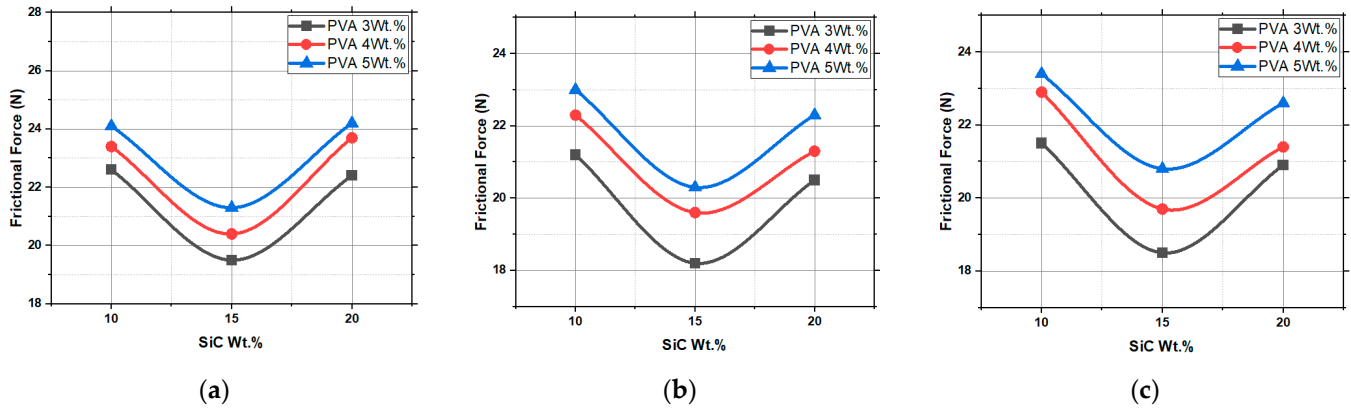

Figure 13. Variation inhardness (BHN) under varying SiC_p (wt.%) and PVA binder (wt.%) with compaction pressure; (**a**) 3 Ton/sq.inch; (**b**) 4 Ton/sq.inch; (**c**) 5 Ton/sq.inch.

The main effects plot (Figure 14) for frictional force indicates that the selection of SiC_p (15 wt.%), compaction pressure (4 ton/sq. inch) and PVA binder (3 wt.%) results in the best combination of input parameters to derive least frictional force values during processing of titaniumcomposites.
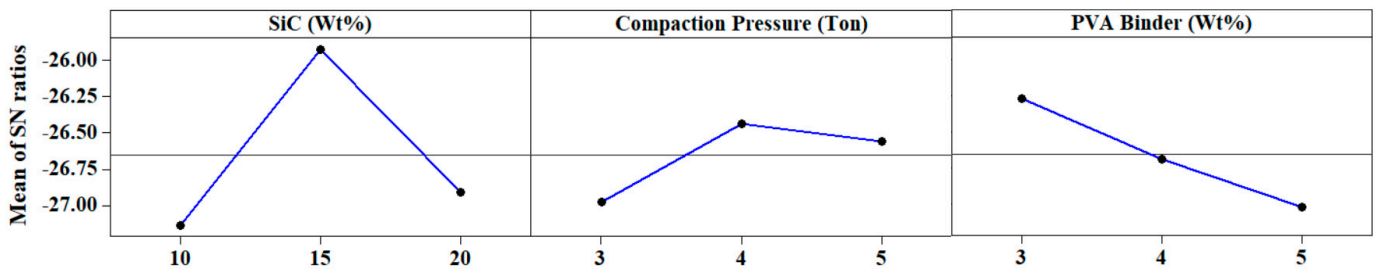

Figure 14. Main effects plot for frictional force (N).

Results of ANOVA deduce that SiC (wt.%) is a prominent factor to be taken into consideration while processing titanium composites. Among the percentage of contribution (P percent) of the various factors (Table 9) for wear, SiC (A) has the largest contribution of around 64.75%. It can be seen that PVA binder (C) ($p = 21.58\%$), compaction pressure (B) ($p = 12.64\%$), and interactions A × B, A × C, ($p = 0.654\%$, 0.244%) had less statistical and physical significance on wear. The interactions (B × C) are not of any physical or statistical significance.

Table 9. ANOVA (analysis of variance) for SN ratios.

Source	Deg.F	Seq. SS	Adj. SS	Adj. MS	F	P	P%
A	2	7.56571	7.56571	3.78286	844.61	0.000	64.75
B	2	1.47715	1.47715	0.73858	164.91	0.000	12.64
C	2	2.52232	2.52232	1.26116	281.58	0.000	21.58
A × B	4	0.15284	0.15284	0.03821	8.53	0.006	0.654
A × C	4	0.05719	0.05719	0.01430	3.19	0.076	0.244
B × C	4	0.02856	0.02856	0.00714	1.59	0.266	0.121
Residual Error	8	0.03583	0.03583	0.00448			
Total	26	11.8396					

Equation (6) presents the second-order differential equation for representing the frictional force(N) which can also be expressed as a function of input processing factors such as (A) SiC (wt.%), (B) compression pressure (Ton/sq. inch) and (C) PVA binder (wt.%).

$$\begin{aligned} \text{Frictional force (N)} = {} & 123.463 - 0.769095\,A - 15.5701\,B - 1.63011\,C + \\ & 0.00392352\,A^2 + 0.652198\,B^2 - 0.147802\,C^2 + 0.00124176\,A \times B + 0.00324176\,A \times \\ & C + 0.556044\,B \times C \end{aligned} \quad (6)$$

Analysis is carried outa significance level of 5% while the level of confidence is at 95%. The results of ANOVA clearly indicate that the 'F' table value (Table 10) is less than the calculated value of 'F' ($F_{(0.05,9,9)}$ = 54.6). Thus, the developed equation is considered adequate.

Table 10. ANOVA for response function of the frictional force (N).

Source	D.F	Seq. SS	Adj. MS	F	P
Regression	9	47.6928	5.2992	54.60	0.000
Residual Error	9	0.8735	0.0971		
Total	18				

For each of the response surfaces, contour and surface plots are plotted at different SiC (wt.%) and PVA binder (wt.%) with compression pressure (4 Ton/sq.inch) is plotted (Figure 15). These response contours and surface plot are used to predict frictional force(N) at any area. It is clear from the figure that the minimum frictional force ranges from 14 to 18 (wt.%) of SiC with 4.5–5 (wt.%) of PVA binder.
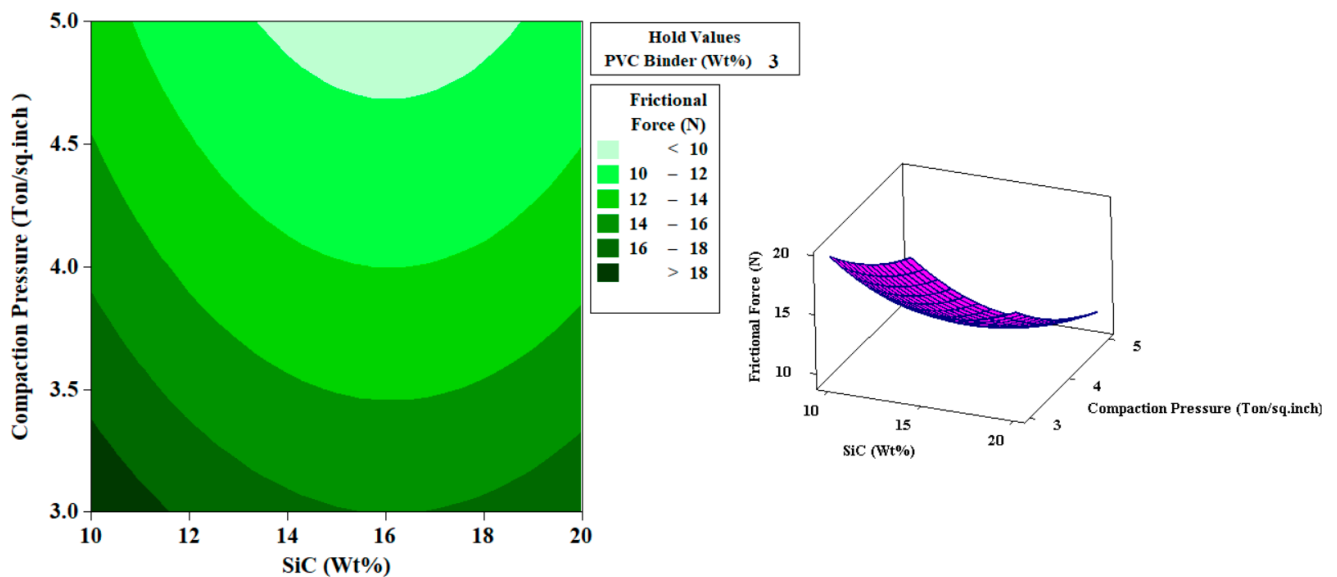
Figure 15. Contour plot and surface plot for frictional force(N).

The RSM predicted values of frictional force(N) are verified by comparing with TDOE values. For 27 trials, the observed average error was 0.47%, which concludes that the estimation is very accurate. Figure 16 presents the verification test results for frictional force(N).
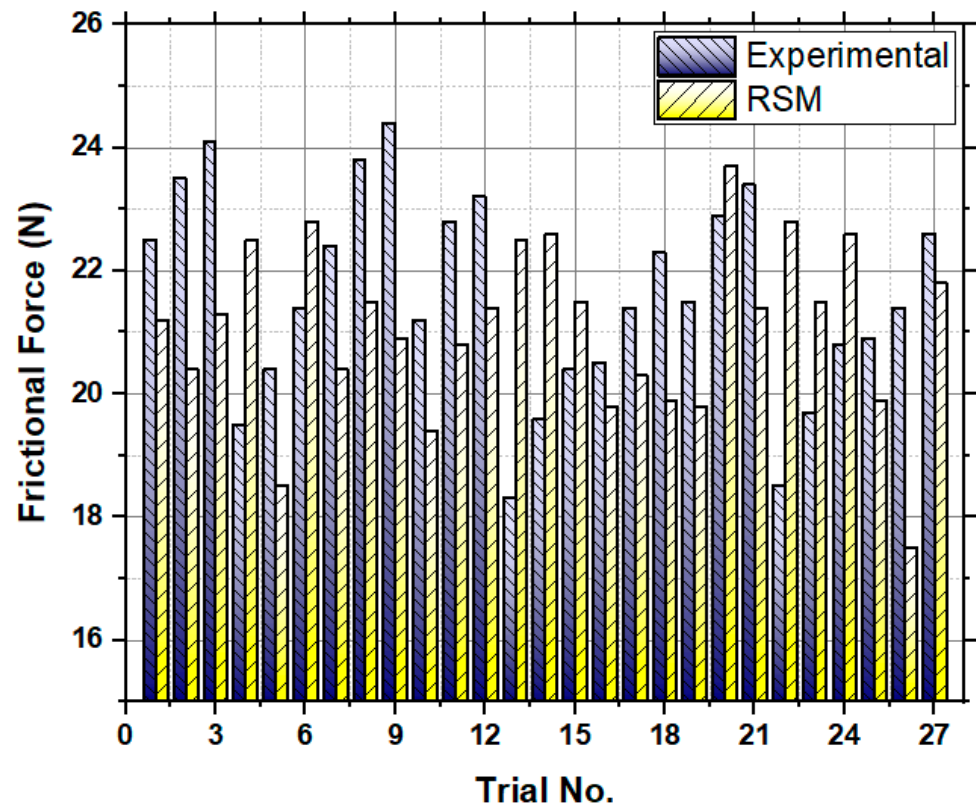
Figure 16. Verification of RSM prediction of frictional force (N).

4. Conclusions

The values of hardness, wear and frictional force of the Ti-6Al-4V-SiC$_p$ composite specimen under various processing conditions using TDOE and RSM are studied. The conclusions drawn based on the results are as follows:

- The SiC (wt.%) is the dominant parameter for the increase in hardness, wear and frictional force, followed by PVA binder (wt.%) and compression pressure (Ton/sq.inch).
- During the fabrication of the Ti-6Al-4V-SiC$_p$ composite specimen, to achieve maximum hardness and minimal wear and frictional force, the factors SiC$_p$ (15 wt.%), compaction pressure (4 ton/sq. inch) and PVA binder (3 wt.%) are preferred.
- From the obtained data, a response surface model of the second order has been created for all the output parameters. Given that the projected and measured values are rather close, it can be used to accurately predict the hardness, wear and frictional force of Ti-6Al-4V-SiC$_p$ composite specimens as they are processed.
- Further, microstructural analysis reveals that 15(wt.%) of SiC$_p$ has resulted in the formation of the α-phase of titanium and silicon carbide, which caused an increase in hardness values compared to 20 (wt.%) of SiC$_p$. With the intermediate SiC content (15 wt.%), the microstructure is optimized, providing a balanced combination of reinforcement and matrix properties reducing the wear and frictional force.
- From atomic force microscopy, it is observed that the 15 wt.% SiC sample reveals a smoother and more controlled surface. The wear behavior at this intermediate SiC content achieves a balance between abrasive and adhesive wear mechanisms, resulting in a relatively more uniform wear profile and reduced surface roughness.
- The findings highlight that in industrial applications involving Ti-6Al-4V-SiCp composites, optimizing the SiC content (15 wt.%), compaction pressure (4 ton/sq. inch), and PVA binder (3 wt.%) can lead to superior hardness, reduced wear, and frictional force, enhancing the overall performance and durability of such composite materials.
- For potential future research, exploring advanced microstructural analyses and surface characterization techniques could further refine our understanding of the relationships

between composition, microstructure, and mechanical properties, allowing for even more precise control and tailoring of composite materials for specific industrial applications.

References

1. Kumar, B.A.; Murugan, N. Metallurgical and mechanical characterization of stir cast AA6061-T6–AlNp. *Compos. Mater. Des.* **2012**, *40*, 52–58.
2. Tzamtzis, S.; Barekar, N.S.; Babu, N.H.; Patel, J.; Dhindaw, B.K.; Fan, Z. Processing of advanced Al/SiC particulate metal matrix composites under intensive shearing—A novel rheo-process. *Compos. Part A Appl. Sci. Manuf.* **2009**, *40*, 144–151. [CrossRef]
3. Tabrizi, S.G.; Babakhani, A.; Sajjadi, S.A.; LÜ, W.J. Microstructural aspects of in-situ TiB reinforced Ti−6Al−4V composite processed by spark plasma sintering. *Trans. Nonferrous Met. Soc. China* **2015**, *25*, 1353–1714.
4. Kimi, Y.; Choim, J.; Kimy, J.; Lee, Y.Z. Friction and wear behavior of titanium matrix (TiB + TiC) composites. *Wear* **2011**, *271*, 1962–1965. [CrossRef]
5. Zhang, Y.Z.; Huang, L.J.; Liu, B.X.; Lin, G.E.N.G. Hot deformation behavior of in-situ TiBw/Ti6Al4V composite with novel network reinforcement distribution. *Trans. Nonferrous Met. Soc. China* **2012**, *22*, 465–471. [CrossRef]
6. Recep, C.; Muharrem, P. The effect of reinforcement volume ratio on porosity and thermal conductivity in Al−MgO composites. *Mater. Res.* **2012**, *15*, 1057–1063.
7. Kok, M. *Production of Metal Matrix (Al₂O₃-Reinforced) Composite Materials and Investigation of Their Machinability by Ceramic Tools*; Firat University: Elazıg, Turkey, 2000.
8. Purazrang, K.; Kainer, K.U. Fracture toughness behavior of a magnesium alloy metal-matrix composite produced by the infiltration technique. *Composites* **1991**, *22*, 456–462. [CrossRef]
9. Ghosh, P.K.; Ray, S. Influence of process parameters on the porosity content in Mg–alumina cast particulate composite produced by vortex method. *Trans. Am. Foundry Soc.* **1988**, *214*, 775–782.
10. Montealegre, M.; Neubauere, A.; Torralba, J.M. Influence of nano-reinforcements on the mechanical properties and microstructure of titanium matrix composites. *Compos. Sci. Technol.* **2011**, *71*, 1154–1162. [CrossRef]
11. Koli, D.K.; Agnihotri, G.; Purohit, R. Properties and characterization of Al−Al₂O₃ composites processed by casting and powder metallurgy routes. *Int. J. Latest Trends Eng. Technol.* **2013**, *2*, 486–496.
12. Usca, Ü.A.; Uzun, M.; Kuntoglu, M.; Şap, S.; Giasin, K.; Pimenov, D.Y. Tribological aspects, optimization and analysis of Cu-B-CrC composites fabricated by powder metallurgy. *Materials* **2021**, *14*, 4217. [CrossRef] [PubMed]
13. Chintada, S.; Dora, S.P.; Kare, D.; Pujari, S.R. Powder metallurgy versus casting: Damping behavior of pure aluminum. *J. Mater. Eng. Perform.* **2022**, *31*, 9122–9128. [CrossRef]
14. Kumar, D.R.; Loganathan, C.; Narayanasamy, R. Effect of glass in aluminium matrix on workability and strain hardening behavior of powder metallurgy composite. *Mater. Des.* **2011**, *32*, 2413–2422. [CrossRef]
15. Gräbner, M.; Wiche, H.; Treutler, K.; Wesling, V. Micromagnetic properties of powder metallurgically produced Al composites as a fundamental study for additive manufacturing. *Appl. Sci.* **2022**, *12*, 6695. [CrossRef]
16. Abdizadeh, H.; Ebrahimifard, R.; Baghchesara, M.A. Investigation of microstructure and mechanical properties of nanoMgO reinforced Al composites manufactured by stir casting and powder metallurgy methods: A comparative study. *Compos. Part B* **2014**, *56*, 217–221. [CrossRef]
17. Chen, R.; Zhang, G. Casting defects and properties of cast A356 aluminum alloy reinforced with SiCp particles. *Compos. Sci. Technol.* **1993**, *47*, 51–56. [CrossRef]
18. Hull, D.; Clyne, T.W. *An Introduction to Composite Materials*, 2nd ed.; Cambridge University Press: Cambridge, UK, 1996.
19. Usca, Ü.A.; Şap, S.; Uzun, M.; Giasin, K.; Pimenov, D.Y. Evaluation of mechanical and tribological aspect of self-lubricating Cu-6Gr composites reinforced with SiC–WC hybrid particles. *Nanomaterials* **2022**, *12*, 2154. [CrossRef]

20. Sap, S.; Turgut, A.; Uzun, M. Investigation of microstructure and mechanical properties of Cu/Ti–B–SiCp hybrid composites. *Ceram. Int.* **2021**, *47*, 29919–29929. [CrossRef]

21. Milan, M.T.; Bowen, P. Tensile and fracture toughness properties of SiCp reinforced Al alloys: Effects of particle size, particle volume fraction, and matrix strength. *J. Mater. Eng. Perform.* **2004**, *13*, 775–783. [CrossRef]

22. Umasankar, V.; Anthony, M.X.; Karthikeyan, S. Experimental evaluation of the influence of processing parameters on the mechanical properties of SiC particle reinforced AA6061 aluminium alloy matrix composite by powder processing. *J. Alloys Compd.* **2014**, *582*, 380–386. [CrossRef]

23. Ghit, C.; Popescu, I.N. Experimental research and compaction behavior modelling of aluminum-based composites reinforced with silicon carbide particles. *Comput. Mater. Sci.* **2012**, *64*, 136–140. [CrossRef]

24. Diler, E.A.; Ipek, R. An experimental and statistical study of interaction effects of matrix particle size, reinforcement particle size and volume fraction on the flexural strength of Al–SiCp composites by P/M using central composite design. *Mater. Sci. Eng. A* **2012**, *548*, 43–55. [CrossRef]

25. George, T.; Rajkumar, R.; Richard, F. Powder Metallurgy Aluminium & Light Alloys for Automotive Applications Conference. In *1 st International Conference on Powder Metallurgy Aluminum & Light Alloys for Automotive Applications*; Jandeska, W.F., Jr., Chernenk, R.A., Eds.; MPIF: Princeton, NJ, USA, 1998; pp. 35–42.

26. Nayak, K.C.; Date, P.P. Development of constitutive relationship for thermo-mechanical processing of Al-SiC composite eliminating deformation heating. *J. Mater. Eng. Perform.* **2019**, *29*, 5323–5343. [CrossRef]

27. Rosso, M. Ceramic and metal matrix composites: Routes and properties. *J. Mater. Process. Technol.* **2006**, *175*, 364–375. [CrossRef]

28. Tan, Z.; Chen, Z.; Fan, G.; Ji, G.; Zhang, J.; Xu, R.; Shan, A.; Li, Z.; Zhang, D. Effect of particle size on the thermal and mechanical properties of aluminum composites reinforced with SiC and diamond. *Mater. Des.* **2016**, *90*, 845–851. [CrossRef]

29. Zeng, X.; Liu, W.; Xu, B.; Shu, G.; Li, Q. Microstructure and mechanical properties of Al–SiCnanocomposites synthesized by surface-modified aluminium powder. *Metals* **2018**, *8*, 253. [CrossRef]

30. Shorowordi, K.M.; Laoui, T.; Haseeb, A.S.M.A.; Celis, J.P.; Froyen, L. Microstructure and interface characteristics of B4C, SiC and Al2O3 reinforced Al matrix composites: A comparative study. *J. Mater. Process. Technol.* **2003**, *142*, 738–743. [CrossRef]

31. Tosun, G.; Kurt, M. The porosity, microstructure and hardness of Al-Mg composites reinforced with micro particle SiC/Al$_2$O$_3$ produced using powder metallurgy. *Compos. Part B* **2019**, *174*, 106965. [CrossRef]

32. Tekmen, C.; Ozdemir, I.; Cocen, U.; Onel, K. The mechanical response of Al-Si-Mg/SiC composite: Influence of porosity. *Mater. Sci. Eng. A* **2003**, *360*, 365–371. [CrossRef]

33. Zhang, J.; Liu, Q.; Yang, S.; Chen, Z.; Liu, Q.; Jiang, Z. Microstructural evolution of hybrid aluminum matrix composites reinforced with SiC nanoparticles and graphene/graphite prepared by powder metallurgy. *Prog. Nat. Sci. Mater. Int.* **2020**, *30*, 192–199. [CrossRef]

34. Poletti, C.; Merstallinger, A.; Schubert, T. Degischer, Materialwissenschaft und Werkstofftechnik. In *Materialwissenschaft und Werkstofftechnik: Entwicklung, Fertigung, Prüfung, Eigenschaften und Anwendungen technischer Werkstoffe*; Wiley-Vch: Weinheim, Germany, 2004; Volume 35, pp. 741–749.

35. Peters, M.; Leyens, C. *Titan und Titanlegierungen*; Wiley VCH: Weinheim, Germany, 2002.

36. Godfrey, T.; Goodwin, P.S.; Ward, C.M. Titanium'99. In Proceedings of the Ninth World Conference of Titanium, Saint-Petersburg, Russia, 7–11 June 1999; pp. 1868–1877.

37. Djanarthany, S.; Viala, J.; Bouix, J. Development of SiC/TiAl composites: Processing and interfacial phenomena. *Mater. Sci. Eng. A* **2001**, *300*, 211–218. [CrossRef]

38. Sap, S.; Uzun, M.; Usca, Ü.A.; Pimenov, D.Y.; Giasin, K.; Wojciechowski, S. Investigation on microstructure, mechanical, and tribological performance of Cu base hybrid composite materials. *J. Mater. Res. Technol.* **2021**, *15*, 6990–7003. [CrossRef]

39. Oh, J.C.; Golkovski, M.G.; Lee, S. Improvement of hardness and wear resistance in SiC/Ti−6Al−4V surface composites fabricated by high-energy electron beam irradiation. *Mater. Sci. Eng. A* **2003**, *351*, 98–108. [CrossRef]

40. Abderrazak, H.; Abdellaoui, M. Synthesis and characterization of nanostructured silicon carbide. *Mater. Lett.* **2008**, *62*, 3839–3841. [CrossRef]

41. Shetty, R.; Hegde, A. Taguchi based fuzzy logic model for optimization and prediction of surface roughness during AWJM of DRCUFP composites. *Manuf. Rev.* **2022**, *9*, 2.

42. Karthik, S.R.; Londe, N.; Shetty, R.; Nayak, R.; Hegde, A. Optimization and prediction of hardness wear and surface roughness on age hardened Stellite 6 alloys. *Manuf. Rev.* **2022**, *9*, 10.

43. Shetty, A.; Hegde, N.T.; Vaz, A.C.; Srinivasan, C.R. A study on the effect of Radiometric Variations on A Fuzzy Stereo Matching Algorithm: A Statistical Analysis. *Eng. Sci.* **2021**, *16*, 269–280. [CrossRef]

44. Shetty, N.; Herbert, M.; Shetty, R.; Shetty, D.S.; Vijay, G.S. Soft computing techniques during drilling of bi-directional carbon fiber reinforced composite. *Appl. Soft Comput.* **2016**, *31*, 466–478. [CrossRef]

45. Shetty, R.; Barboza, A.B.V.; Kini, L.G. Empirical study on stress distribution zone during machining of dracs using finite element analysis, taguchi's design of experiments and response surface methodology. *ARPN J. Eng. Appl. Sci.* **2022**, *14*, 2576–2582.

46. Shetty, R.; Kumar, S.; Mallagi, R.; Keni, L. L16 Orthogonal Array-based Three-Dimensional Finite Element Modeling for cutting force and chip formation analysis during dry machining of Ti-6Al-4V. *J. Adv. Manuf. Syst.* **2021**, *20*, 123–134. [CrossRef]

47. Shetty, R.; Gurupur, P.R.; Hindi, J.; Hegde, A.; Naik, N.; Ali, M.S.S.; Patil, I.S.; Nayak, M. Processing, Mechanical Characterization and Electric discharge machining of Stir cast and Spray forming based Al-Si alloy reinforced with ZrO$_2$ particulate composites. *J. Compos. Sci.* **2022**, *6*, 323. [CrossRef]
48. Hegde, A.; Shetty, R.; Chiniwar, D.S.; Naik, N.; Nayak, M. Optimization and Prediction of Mechanical Characteristics on Vacuum Sintered Ti-6Al-4V-SiC$_p$ composites using Taguchi's Design of experiments, Response Surface Methodology and Random Forest Regression. *J. Compos. Sci.* **2022**, *6*, 339. [CrossRef]